To be published, *Journal of Directed Energy*

Evaporation and Beam Profile Measurements on an Irradiated Water Drop

Timothy E. Tracey and Cody J. Brownell*

Mechanical Engineering Department, United States Naval Academy, Annapolis, Maryland 21402

This work investigates the interaction of a high energy laser and single water drops. The drop thermodynamics and optical propagation of the laser are coupled through the absorption-dependent vaporization process. An analytical model of absorption and rapid evaporation for small aqueous aerosols is extended for use with large drops. Experimentally, a high energy infrared laser is used to irradiate single drops of water, and the drop shape and size as well as the transmitted beam profile are measured. The drop is levitated using an ultrasonic levitator, where the drop is held in place by the pressure from a standing sound wave. Drop size and composition are varied, along with the incident laser power. Experimental data are used to validate findings from the analytical model, and to show the effects of drop size, composition, and irradiance on evaporation rate. An overall energy balance for the drop is discussed, and the relative magnitude of absorption, transmission, and reflection are estimated from the data. Several qualitative observations are used to suggest areas for further work.

KEYWORDS: Raindrop, Vaporization, HEL, Imaging

Nomenclature

ρ	density
C_p	specific heat
R	drop radius
D	drop diameter
T	temperature
K	thermal conductivity
v	velocity
h_{fg}	enthalpy of vaporization
M	mass
Q_{abs}	absorption efficiency
I_o	irradiance
α	absorptivity
e	ellipticity

Received May 15, 2017; revised January 5, 2018.
*Corresponding author email: brownell@usna.edu.

a	major radius of spheroid
c	minor radius of spheroid
V	volume

Introduction

The complexity of a maritime environment imposes particular challenges for laser propagation. With high energy laser (HEL) weapons, liquid water droplets from fog, rain, or sea spray can interfere with transmission.[1] On the defensive side, the observed challenges to laser weapons imposed by liquid water present an opportunity; it may be possible for a small watercraft or a drone to hide in rain, clouds, or the like.

Characterization of the maritime environment and simulation of laser propagation through this environment is an active area of research. This includes the development of tools to model atmospheric constituents or conditions such as the Advanced Navy Aerosol Model (ANAM),[2] and atmospheric propagation and characterization codes such as the Laser Environmental Effects Definition and Reference (LEEDR). Specifically, LEEDR contains a number of rain rate variations, each with specified drop-size distributions, where the drops are modeled optically as spheres.[3,4] The code can evaluate forward and off-axis scattering, and molecular absorption effects on electromagnetic propagation over a range of wavelengths. To simulate high-energy physical processes and interactions, tools such as the High Energy Laser Code for Atmospheric Propagation (HELCAP), developed by the Navy Research Laboratory (NRL), can model thermodynamic processes such as heating and vaporization of aerosols and thermal blooming.[5] Developed by the Air Force Institute of Technology's (AFIT) Center for Directed Energy, the High Energy Laser End-to-End Operational Simulation, or HELEEOS, is able to leverage LEEDR and other codes into a probabilistic outcome of an HEL engagement scenario, including certain nonlinear atmospheric heating effects.[6,7]

Despite the vigorous research activity described above, the interactions between a high energy laser and large liquid water drops, such as rain or sea spray, are not clear. An important contrast must be made between small, aqueous aerosol "droplets," with diameters less than approximately 100 μm, and large water "drops," like rain, that may have a diameter of several millimeters. In both cases, the drop thermodynamics and the optical propagation of the laser are coupled through the absorption-dependent vaporization process. However, the large size of the drops results in fundamental changes to both optical propagation and thermofluid phenomena within the drop. Most important is the diminished role of the liquid's viscosity; in large drops the momentum forces within the fluid, driven by localized heating and buoyancy effects, will exceed the viscous forces. When this happens turbulent eddies will form within the drop, advection will dominate heat diffusion, and the drop temperature will vary rapidly both spatially and temporally. The net effect of this is that temperature (however it is characterized) in large drops is difficult to predict, and temperature-dependent processes like evaporation are similarly affected.

Absorption in water depends strongly upon impurities within the water, and it is difficult to predict absorption *a priori* for a given sample. Pure seawater consists of water and various dissolved salts, on the order of 35 parts per thousand by weight.[8] The salts in seawater have a negligible effect on absorption except at very long wavelengths; the effect of salts on scattering is more significant. For IR radiation in seawater, phytoplankton is the primary par-

ticulate that determines optical properties, at lengths of 1 to 200 μm.[8] Chlorophyll and related pigments found in phytoplankton are strong absorbers, and overall, the absorption of a water sample is highly dependent on its concentration of particulates like phytoplankton.

Previous experimental research on droplet heating with lasers has typically used CO_2 lasers, which produce a 10-micron wavelength. The absorptivity of liquid water at this wavelength is high, so heating effects can be drastic. Heating of small aqueous aerosols with CO_2 lasers found two distinct heating regimes, a "slow" regime where the heat led to rapid evaporation of the droplet and a "fast" regime where a single laser pulse resulted in explosive vaporization.[5,9–13] Other work investigated the effects of irradiated droplets for the application of cloud clearance, using droplets with diameters from 1–140 μm.[14] For drops greater than 100 μm in diameter, single-drop experiments with liquid fuels have been conducted with combustion-related applications, but little else can be found in the literature.[15–16]

Theory

Comparing the heating of a large drop (1-mm diameter) to small aqueous aerosols, three key assumptions for aerosol heating need to be re-assessed: (1) use of a Mie absorption efficiency, (2) isothermal drop, and (3) uniform heating. In light of this, we wish to explore the extent to which analytical results from radiatively heated aerosols may be applied to larger water drops. To begin, see energy conservation applied to an aqueous aerosol droplet, using the form found in Davies and Brock[17]:

$$\begin{aligned}\rho_D C_{pD} 4/3\pi R^3 dT_D/dt + 4\pi R^2 \rho_D C_{pD} dR/dt \\ = 4\pi R^2 \left[K_g (dT/dR)|_R - (\rho_g v_g C_{pg} T_g)|_R - 1/2 \rho_a v_a^3\right] + h_{fg} dM/dt \\ + \pi R^2 Q_{abs} I_o\end{aligned} \quad (1)$$

where ρ is density, C_p is specific heat, R is drop radius, T is temperature, v is velocity, h_{fg} is enthalpy of vaporization, M is mass of the drop, Q is an absorption efficiency, and I_o is the laser irradiance. The subscript D is for the drop, g is for the host gas, and a is for the vapor. The two terms on the left side of the equation represent changes to energy stored within the drop due to sensible heating. The three terms in brackets on the right side account for energy transfer through the surface of the drop due to conduction, bulk convection of host gas, and vapor kinetic energy, respectively. The last two terms in Eq. 1 are for latent heat loss and energy absorbed from the laser.

The application of the equation above will extend to larger water drops, assuming C_p is an integrated drop temperature and that Q_{abs} is treated appropriately. In prior analyses, Q_{abs} is the Mie absorption efficiency and is assumed to be proportional to drop radius when $D < 32\ \lambda$.[18] The radiation absorption term is then written as

$$\pi R^2 Q_{abs} I_o = 4/3\pi R^3 \alpha I_o \quad (2)$$

where α is the bulk absorption coefficient. This condition is not satisfied for millimeter-sized drops with any laser source. The Mie absorption coefficient arises geometrically from assuming an optical path length equal to the average thickness of a sphere, 4/3 R. For a water drop in air that exceeds the Mie limit and is in the geometric regime, refraction and attenuation of the light through the body may be relevant. Still, linear dependence on R may be assumed for all cases where attenuation is small. The analysis here continues

with $Q_{abs} = 4/3\ R\alpha$, while recognizing that this may slightly underestimate the absorbed radiation.

For the case where thermal conduction can be neglected, Eq. 2 gives a quasi–steady-state relationship between irradiation and vaporization rate. According to Williams,[19]

$$-h_{fg}\,dM/dt = 4/3\pi R^3 \alpha I_o \tag{3}$$

Writing $dM/dt = \rho_D\, 4\pi R^2\, dR/dt$, Eq. 3 can be recast as

$$dR/dt = -\alpha I_o R/3\rho_D h_{fg} \tag{4}$$

with the following solution for $R(t)$:

$$R = R_o\, exp[-(\alpha I_o/3\rho_D h_{fg})\, t\,] \tag{5}$$

Williams,[19] while holding to the three initial assumptions, stated that Eq. 5 is valid for millimeter-sized drops and larger, assuming that the absorbed radiant energy flux is not so large as to make the vapor kinetic energy important. If the quasi–steady-state vaporization rate is set strictly through Eq. 5, Williams[19] argues that the drop surface temperature is determined by the evaporation rate through the Hertz-Knudsen equation. With a large drop, however, the interface is far from isothermal and the surface temperature is affected by advection of hot eddies from the interior of the drop to the surface. Because diffusive mechanisms, while important, do not dominate the interior drop dynamics, both spatial and temporal fluctuations in surface temperature are expected. The way that this dynamic drop interface affects the rapid evaporation of the water is not well understood; a full model would require a solution to both the Navier-Stokes equations and the scalar transport equation for temperature within the entire drop.

Experiment

To validate the use of a simplified equation for vaporization rate for large water drops and to investigate other possible influences on drop temperature or vaporization rate that are unique to large drops, a series of experiments involving acoustically levitated, irradiated drops is presented.

Figure 1 shows a schematic of the overall experimental setup, located at the Naval Academy's Directed Energy Research Center (DERC). The drops in this experiment were suspended by a tec5 AG ultrasonic levitator. This levitator produces four to five pressure nodes, but only two to three can be used for stable levitation.[20] The size of the drops levitated depends on the wavelength of the sonic wave used to create the pressure nodes. The optimal drop diameter is given as $d_s = \lambda/3$, where λ is the acoustic wavelength, as this is the diameter that requires the minimum power to levitate the drop. The standard operating parameters for the levitator are an acoustic wavelength of about 5.9 mm and a frequency of 58 kHz, making the optimal drop size approximately 2 mm. In these experiments, drop size did not exceed 2.5 mm, using mid-range power while creating a stable platform for droplet levitation. The acoustic energy density profile surrounding the levitated drop causes the drop to deform and take on an oblate spheroid appearance. This is a result of the balancing of capillary and gravitation forces experienced by the drop during its levitation. In practice, the ellipticity $e = [1 - c^2/a^2]$ of drops varied from 0.7 to 0.99, with higher ellipticities (rounder drops) at smaller sizes. This is actually a smaller range than seen in raindrops, which can vary in size and shape dramatically and will often oscillate while falling.[21]

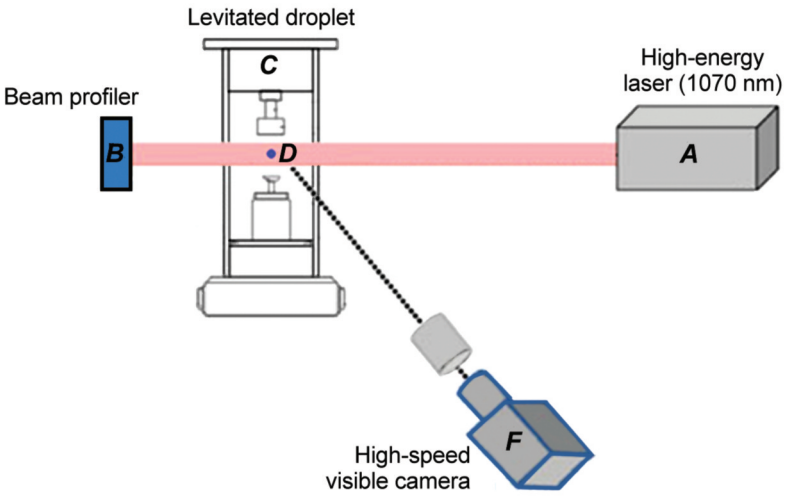

Fig. 1. Experiment schematic.

The laser used in this experiment is a 100-W IPG Photonics high-power fiber laser. The output beam power and profile were measured before the experiments to confirm specifications. The laser output at full power was 107 W, and the maximum $1/e^2$ beam diameter at the target was 5.28 mm. Because the drops used in these experiments are smaller than the beam diameter, the average irradiance incident upon the drop is larger than the mean irradiance value, and will change by ~5% as the drop vaporizes and shrinks. The peak intensity for a Gaussian beam with these characteristics is 977 W/cm^2, and 900 W/cm^2 is a representative value for irradiance incident on the drop at full power. Beam data are collected after a beam splitter via a Spiricon SP620U, with a 1600 × 1200 pixel resolution and capable of 7.5 frames per second at full resolution, and with a thermopile for integrated power. High-resolution video of the drop evaporation process is captured with a Hamamatsu ORCA-Flash2.8 camera using a Navatar macro lens. In addition to the equipment shown in the schematic, a Jasco V-670 Model ISN-723 integrating sphere was used to determine absorptivity for the water samples tested.

Because drop images contain no external reference, image resolution had to be independently calibrated in order to extract accurate diameters. This was done by placing a 5/64-in (1.985-mm) rod within the camera field of view, and measuring the pixel count across the rod. An uncertainty of 1 pixel is assumed in locating the gradients in the image for the pixel count, making the calibration error in reported length measurements approximately ±0.01 mm.

Data were collected for over 90 runs, each with a unique drop placed in the levitator and lased for up to 60 s. The initial drop size, water source, and incident power were all varied. Data reduction processes used MatLab's Image Processing Toolbox to decompose drop video data into measurements of the major and minor axes of the drop at a given frame. A sample drop image is shown in Fig. 2. Drop mass and/or volume was then computed by assuming symmetry about the vertical axis, $V = 4/3\pi a^2 c$ where a is the major (horizontal) radius and c is the minor (vertical) radius.

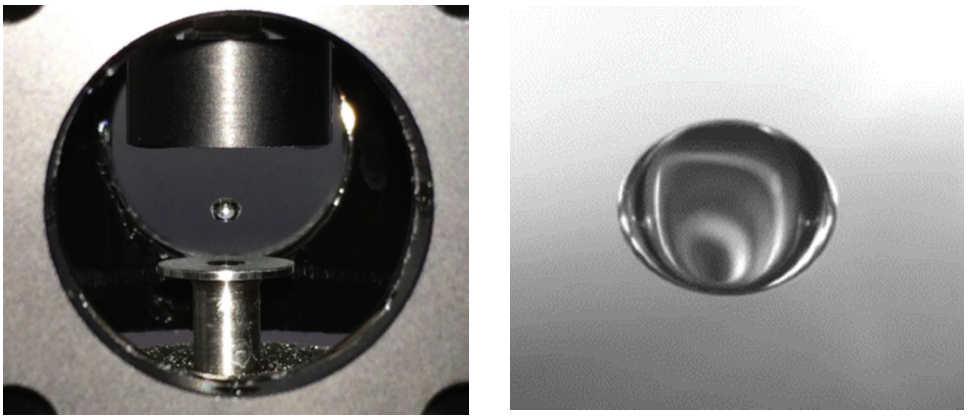

Fig. 2. Drop in levitator (left), and drop image from Hamamatsu camera (right). Drop diameter approximately 1.5 mm in both images.

Results

Sample results for droplet volume versus time are shown in Fig. 3. The figure shows data from eight nominally identical tests. In each run shown in the figure, the drop was placed in the levitator using a pipette set at 0.0015 mL (1.5 mm^3) and exposed to a 107-W beam. The run-to-run consistency demonstrates the repeatability of the experiment and provides insight into the evaporation process. Each "run" in the figure corresponds to an evaporation process of an individual water drop, where all drops were taken from the same source. These results suggest that there were no significant differences in absorptivity from sample to sample, and no alignment irregularities between the beam and the drop. Data points that appear as outliers are due to temporary instabilities of the drop within the levitator, which result in blurred images and in difficulty in extracting the major and minor diameters from the images.

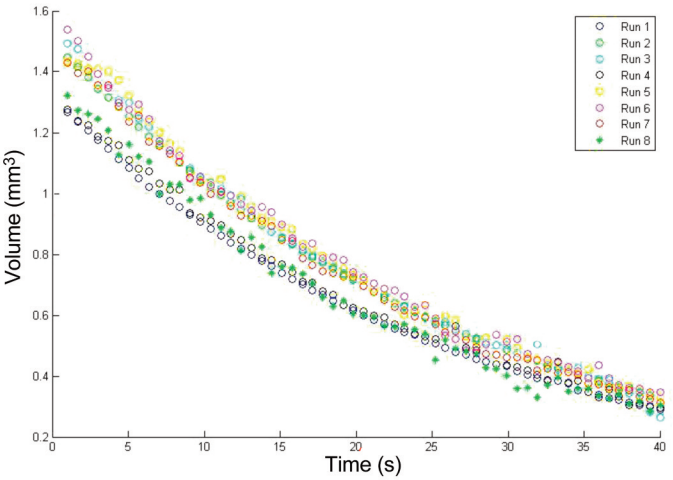

Fig. 3. Drop volume vs time, showing experiment repeatability.

Qualitatively, it is notable that the drop begins shrinking to within the resolution of our measurements, immediately upon initiation of the laser strike. This suggests that any initial period of sensible heating is quite brief and the vaporization process begins rapidly. Because the drops are initially at room temperature, some delay between initial irradiation and observable phase change was expected for either evaporation or bulk vaporization mechanisms. While the primary phase change mechanism appears to be rapid evaporation, some anecdotal evidence suggests, at least in some cases, concurrent nucleate boiling. High-speed video on occasion shows what appear to be very small vapor bubbles bursting through the top surface of the drop. Video has also picked up structures within the drop that appear to be vortex lines formed by small bubbles accumulating in the low-pressure vortex core. While these bubbles could be dissolved gases that were present in the initial sample, they could also be from vaporization of the liquid. Neither of these observations is conclusive, but further investigation into a nucleate boiling regime is warranted.

Figure 4 on the left shows the effect of incident laser power on vaporization rate. This supports the assertion above that the decay constant from Eq. 5, describing the reduction of drop size with time, is proportional to incident irradiance. On the right, measurements of drop volume versus time are plotted against the predicted vaporization rate. In the figure, the model uses an enthalpy of vaporization $h_{fg} = 2256 \frac{kJ}{kg}$, a density of $\rho = 1000$ kg/m^3, a mean irradiance of $I_o = 8 \times 10^6$ W/m^2, and an absorptivity of $\alpha = 0.1225$ cm^{-1}. The decay constant in the exponential is then $\alpha I_o / 3 \rho h_{fg} = 0.0145\ s^{-1}$. Note that the sample absorptivity has been adjusted in the plot compared to measured absorptivity of $\alpha = 0.14$ cm^{-1}. The lower value provides the best fit to the data in this case, and sample-to-sample variations in α of this magnitude are not unexpected. In either case, the model appears to be a good fit to the measured data over the parameter space tested.

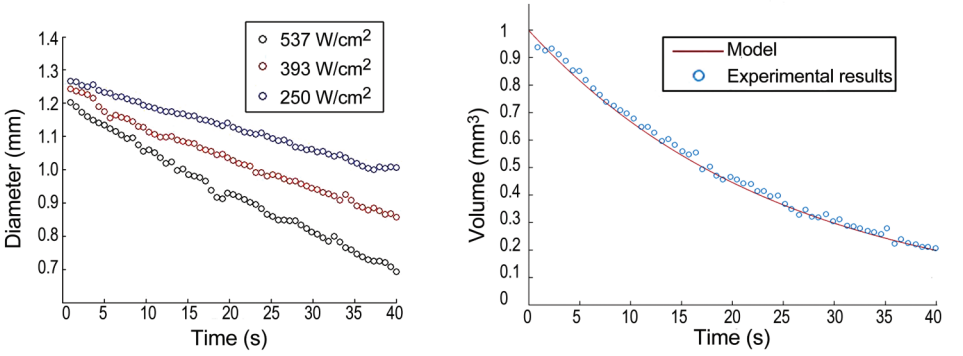

Fig. 4. Effect of irradiance on evaporation rate (left) and comparison of model to experimental results (right).

For cases where the energy balance in Eq. 3 is valid, that is, where the absorbed energy is required to balance with a rate of phase change and conduction can be neglected, then measurements such as those above may be used to calculate the absorptivity of a sample a posteriori. This is a more direct measurement of the property than typical absorption spectroscopy, where transmitted energy is measured to deduce absorption.

To further assess the transmitted and reflected radiation from the drop, power and beam profile measurements were obtained for several of the drop samples. Fig. 5 shows at left a

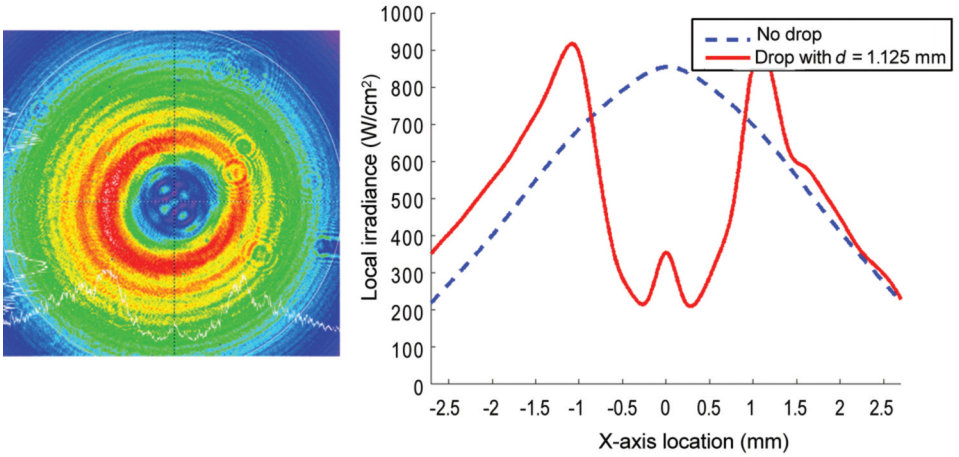

Fig. 5. BeamGage image of 1.125-mm drop (left) beam profile of same, compared to beam without drop (right).

sample beam profile image with a 1.125-mm drop in the beam path, and at right the corresponding beam profile of the same drop, compared to the incident beam profile. In both, the shadow cast by the drop is clear. Interestingly, diffraction effects are also pronounced. An Arago spot is visible in most beam profile images with the drop in place. The beam profile at right shows a single bright spot, but visible in the image at left there are actually several spots within the shadow. These appear due to the ellipticity of the sphere, and therefore change with both drop size and shape.

A final variable of interest is the effect of the water sample on vaporization rate. To explore this, several experiments were conducted comparing vaporization of distilled water to water samples obtained from the Chesapeake Bay near the mouth of the Severn River. Chesapeake Bay water is brackish, and likely contains organic material that may vary from sample to sample. The apparatus used to measure absorptivity of the water samples has an experimental photometric uncertainty greater than the measured difference between the two samples. The distilled water sample absorption coefficient was measured to be approximately 0.148 cm^{-1}. In comparison, the measurements for the natural water sample varied from 0.12 cm^{-1} to 0.17 cm^{-1}; in further experiments, it will be necessary to devise an alternative method for determining this absorptivity. The focus here is on the behavior of the droplet when comparing a pure sample to an impure sample. In practice, an operational HEL will experience contact with water varying in salinity and turbidity, and therefore the comparison is useful in seeing whether or not a significant effect results from an impure sample.

Figure 6 shows comparisons of drop diameter vs time for both distilled and natural (brackish) water, with two different initial drop sizes. In the smaller droplet ranges, the decay rate for distilled and turbid water is very similar. At a drop size of 1.25 mm the brackish water sample vaporizes slightly slower. With the larger drop size, the effect is more pronounced. The difference between distilled and brackish sample vaporization rates for a 1.75 mm drop diverge significantly, and this divergence appears to increase as lasing continues.

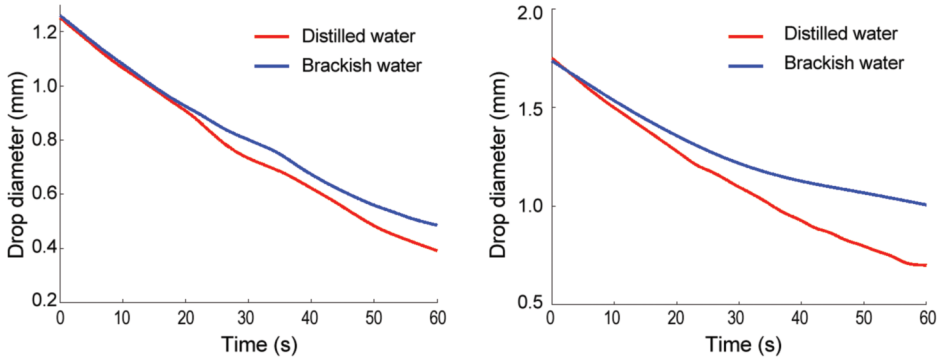

Fig. 6. Diameter vs time for distilled (left, d = 1.25 mm) vs brackish water (right, d = 1.75 mm).

During the final 30 s of the laser strike, the brackish sample shows surprising resilience to phase change. One possible explanation for this behavior is that the impurities in the water sample become more concentrated as the liquid evaporates, and they begin to interfere with the evaporation process at the liquid surface. This may be a case where the assumptions in equation (3) are no longer valid, if the balance between absorption and vaporization rate does not hold in this case. The qualitative differences in vaporization rate between the two water samples suggests that this needs further study.

Analysis and Discussion

To form a better understanding of the coupled optics and drop thermodynamics, energy balances are computed for the drop as a function of lasing time using data collected from both the beam profiler and the high-speed camera. Table 1 provides power meter readings for the beam with no drop present, and with the presence of two different drop sizes. These powers are compared to the total power from the Gaussian beam incident on an aperture with size equal to the projected area of the drop. For the smaller 1.125-mm diameter drop, 8.7% of the beam power (9.3 W) is incident upon the drop, and the reduction in measured

Table 1. Beam Power and Attenuation

	Total incident power	107 W
Small drop D = 1.125 mm	Measured power	100.7 W
	Reduction in power	5.8%
	Beam power through aperture	8.7%
	Maximum local irradiance reduction	73.9%
Large drop D = 1.75 mm	Measured power	92.8 W
	Reduction in power	13.3%
	Beam power through aperture	19.7%
	Maxium local irradiance reduction	79%

power at the meter is 5.8% (6.2 W). With the larger 1.75-mm drop, the corresponding numbers are 19.7% incident and 13.3% reduction in measured power. The difference between these numbers, approximately one third of incident power in both cases, provides an estimate of the transmitted power through the drop. The measured reduction in power is due to a combination of absorption and reflection (with some scattering), with reflection accounting for the majority of attenuated power.

Looking at the attenuated beam power, the relative effects of absorption and reflection can be visualized for irradiated drops of different sizes. The expectation is that reflected power will scale with area as R^2, while absorbed power will scale with volume as R^3. Larger drops should produce proportionally more absorption than reflection, and the fraction of power reflected should increase as the drop vaporizes and shrinks. For all cases in this regime, the magnitude of reflected power will be significantly greater than absorbed power. With this assumption, a representative value of reflected power is determined from beam power and profile measurements. This value comes from the attenuated power measured by the power meter and is here assumed to be equal to reflected power, without subtracting the absorption estimate. In Figs. 7 and 8, this estimate of reflected laser power is compared to the power required to produce the measured rate of phase change, in red, and also to calculations of maximum possible power loss through thermal conduction/convection, in light blue. The convective loss is derived from a Nusselt number for free convection from small spheres, and by assuming the drop is at saturation temperature. While the mean surface temperature of the drop is likely well below the saturation temperature, this assumption provides an upper bound for convective heat loss. Note the axis scale used for reflected power has been adjusted for visualization purposes.

Figures 7 and 8 both show how the constituent effects of the drop on the laser vary with drop size and lasing time. For small drops, conduction and/or convection from the drop to the surrounding medium has increased importance compared to other energy dissipation mechanisms. At the end of the laser strike for the 1.125-mm drop, the drop diameter was approximately 0.6 mm, which begins to approach the small droplet regime covered in

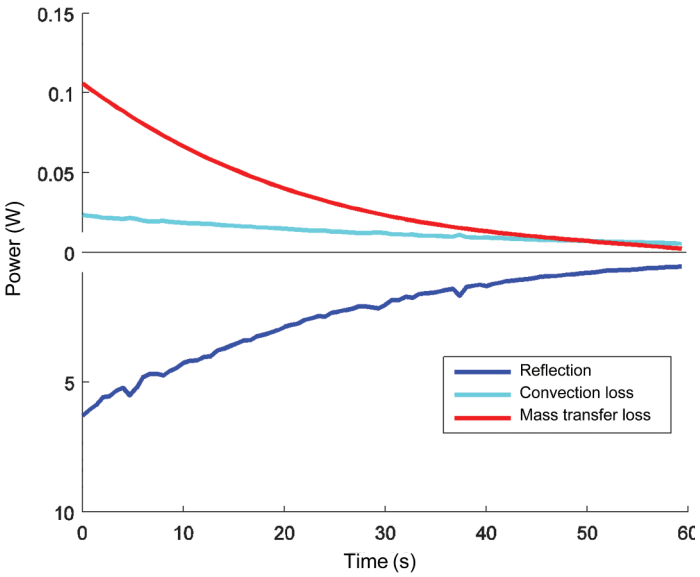

Fig. 7. Laser power interactions for 1.125-mm diameter drop. Above axis, laser power absorbed that leaves drop due to mass transfer (phase change) or conduction/convection with surroundings. Below axis, attenuation at power meter due primarily to reflection from drop. Note different scales above and below the axis.

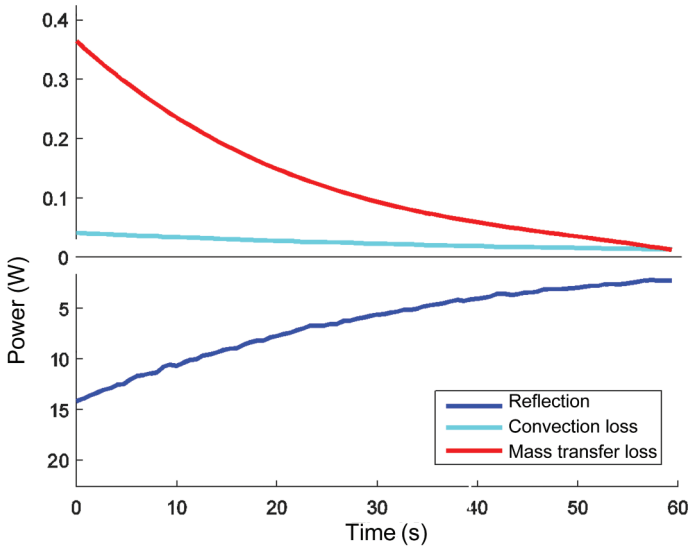

Fig. 8. Laser power interactions for 1.75-mm diameter drop. Note different scales above and below axis.

other work. While Fig. 7 shows the magnitude of power dissipation from convection actually exceeding that from phase change, in reality the drop temperature will be much lower than the saturation temperature used in these calculations, so this is unlikely to be the case. Looking at the data for both the large and small drop, there is a much more substantial change from the beginning to the end of the laser strike above the axis, in the power absorbed, than below the axis, in power reflected. This confirms the expectations stated above, that absorbed power, and therefore vaporization rate, will scale as R^3 vs an R^2 scaling for reflection. Extrapolating these trends to larger drops, 5% of attenuation from a 3.5-mm diameter raindrop would be due to absorption versus reflection.

Conclusions

A series of experiments was successful in exploring the coupling between a large water drop and a high energy laser. Data collection took place using a high-speed visible camera in conjunction with a beam profiler and power meter. The combination of these devices allowed for concurrent characterization of a water drop and a HEL, and the experiment as a whole served as a proof of concept for the utility of levitated drop experiments to the directed energy community.

Several conclusions may be drawn from the data. Predicted vaporization rates, based on a balance between absorbed radiation and the rate of phase change, appear to hold for the range of parameters tested. While qualitative observations suggest vigorous mixing and turbulence within the drop, this does not appear to affect the vaporization rate. Irradiation of natural water drops taken from Chesapeake Bay showed stunted vaporization rates, particularly in the latter half of the laser strike. This may be due to increasing concentrations of impurities, but the mechanism for this is unclear. The power on target for a laser passing through rain is dominated by reflection from the drops, but it will have a larger absorption component as the drop size increases.

In an actual HEL engagement scenario, effects of the water vapor released from the drop on the path of the laser are unknown, and convective heating of the air around the drop may lead to increased scintillation. Nucleation and the formation of vapor pockets on impurities within the drop may significantly alter the interior drop geometry as well, resulting in additional deformation and refraction. The conditions under which nucleate boiling will occur and the effects this has on relevant processes need to be examined further. Related to the onset of nucleate boiling, the drop temperature distribution is also unknown. Because calculations of drop temperature may require a Navier-Stokes solution within the drop, predictions of either instantaneous or mean drop temperature may prove difficult.

Acknowledgments

The authors are grateful for support from the ONR Counter-Directed Energy Weapons Program (Ryan Hoffman and Peter Morrison), HEL-JTO (Harro Ackermann), DEPS (Mark Neice), and the USNA Trident Scholar Program (Reza Malek-Madani and Maria Schroeder).

References

1. O'Rourke, R., Navy shipboard lasers for surface, air, and missile defense: Background and issues for Congress, Congressional Research Service (2014).
2. van Eijk, A.M.J., Merritt, D.L., Improvements in the Advanced Navy Aerosol Model (ANAM), Proc. SPIE 6303, Atmospheric Optical Modeling, Measurement, and Simulation II, 63030M, September (2006), doi: 10.1117/12.680295.
3. Fiorino, S.T., Bartell, R.J., Krizo, M.J., Caylor, G.L., Moore, K.P., Harris, T.R., Cusumano, S.J., Proc. SPIE, **6878**, 68780B (2008).
4. Fiorino, S.T., Randall, R.M., Via, M.F., Burley, J.L., J. Appl. Meteorol. Climatol., **53**, 1 (2014).
5. Sprangle, P., Peñano, J., Hafizi, B., Optimum wavelength and power for efficient laser propagation in various atmospheric environments, report NRL/MR/6790-05-8907 (2005).
6. Fiorino, S.T., Bartell, R.J., Perram, G.P., Bunch, D.W., Gravley, L.E., Rice, C.A., Manning, Z.P., Krizo, M.J., J. Directed Energy **1** (2005).
7. Air Force Institute of Technology, Center for Directed Energy, HELEEOS, https://www.afit.edu/cde/ (accessed 2017).
8. Mobley, C., Optical properties of water. In Bass, M., Ed., *Handbook of Optics* , 2nd ed. McGraw Hill (1994).
9. Zardecki, A., Armstrong, R.L., Appl. Opt. **27**, 17 (1998).
10. Armstrong, R.L., Park, B.S., Appl. Opt. **28**, 17 (1989).
11. Armstrong, R.L., O'Rourke, P.J., Zardecki, A., Physics Fluids **29**, 11 (1986).
12. Armstrong, R.L., Appl. Opt. **23**, 1 (1984).
13. Carls, J.C., Brock, J.R., Aerosol Sci. Technol. **7** (1987).
14. Kafalas, P., Herrmann, J., Appl. Opt. **12**, 4 (1973).
15. Saha, A., Basu, S., Kumar, R., Exp. Fluids **52** (2012).
16. Saha, A., Basu, S., Kumar, R., Appl. Phys. Lett. **100**, 204104 (2012).
17. Davies, S.C., Brock, J.R., Appl. Opt. **26**, 5 (1987).
18. Jacobson, M., *Fundamentals of Atmospheric Modeling*, Cambridge University Press (2005).
19. Williams, F.A., Intl. J. Heat Mass Transfer **8** (1965).
20. Basics about ultrasonic levitation, in *Ultrasonic Levitator Manual*, Tec5-Technology for Spectroscopy (2014).
21. Beard, K.V., Bringi, V.N., Thurai, M., Atmosph. Res. **97**, 4 (2010).